nature genetics

Lamr1 functional retroposon causes right ventricular dysplasia in mice

Yoshihiro Asano[1], Seiji Takashima[1], Masanori Asakura[1], Yasunori Shintani[1], Yulin Liao[1], Tetsuo Minamino[1], Hiroshi Asanuma[1], Shoji Sanada[1], Jiyoong Kim[2], Akiko Ogai[2], Tomi Fukushima[1], Yumiko Oikawa[1], Yasushi Okazaki[3], Yasufumi Kaneda[4], Manabu Sato[4], Jun-ichi Miyazaki[5], Soichiro Kitamura[2], Hitonobu Tomoike[2], Masafumi Kitakaze[2] & Masatsugu Hori[1]

Arrhythmogenic right ventricular dysplasia (ARVD) is a hereditary cardiomyopathy that causes sudden death in the young. We found a line of mice with inherited right ventricular dysplasia (RVD) caused by a mutation of the gene laminin receptor 1 (*Lamr1*). This locus contained an intron-processed retroposon that was transcribed in the mice with RVD. Introduction of a mutated *Lamr1* gene into normal mice by breeding or by direct injection caused susceptibility to RVD, which was similar to that seen in the RVD mice. An *in vitro* study of cardiomyocytes expressing the product of mutated *Lamr1* showed early cell death accompanied by alteration of the chromatin architecture. We found that heterochromatin protein 1 (HP1) bound specifically to mutant LAMR1. HP1 is a dynamic regulator of heterochromatin sites, suggesting that mutant LAMR1 impairs a crucial process of transcriptional regulation. Indeed, mutant LAMR1 caused specific changes to gene expression in cardiomyocytes, as detected by gene chip analysis. Thus, we concluded that products of the *Lamr1* retroposon interact with HP1 to cause degeneration of cardiomyocytes. This mechanism may also contribute to the etiology of human ARVD.

ARVD is a type of right ventricular cardiomyopathy characterized by the gradual loss of cardiomyocytes and compensatory replacement with either adipose or fibrous tissue. ARVD is a primary cause of sudden cardiac death in juveniles and athletes, but is difficult to diagnose before the onset of cardiac events. In Italy, ARVD accounts for 20% of all sudden deaths in individuals under 35 years old and 22% of sudden deaths in athletes[1]. The etiology of this disease is still unknown. Familial occurrence is reported in about 30% of individuals with ARVD. Six associated loci have been mapped: ARVD1, 14q23 (ref. 1); ARVD2, 1q42 (ref. 1); ARVD3, 14q12 (ref. 2); ARVD4, 2q32 (ref. 3); ARVD5, 3p23 (ref. 4); and ARVD6, 10p12 (ref. 5). The only gene identified so far is that underlying ARVD2, which corresponds to the cardiac ryanodine receptor gene and causes a condition with different features from those of the other forms of ARVD[6]. As in humans, a naturally occurring phenotype of RVD has been reported in dogs, cats and minks[7–10], but the genes responsible have not been identified.

We report here a new mouse model of ARVD: we identified a retroposon insertion encoding a mutant form of the nuclear protein laminin receptor 1 (LAMR1) by positional cloning. LAMR1 is one of the ribosomal proteins localized in the nucleus and involved in apoptosis[11,12]. We also report possible molecular mechanisms leading to ARVD.

RESULTS

Mouse model of ARVD

We found a mouse model of ARVD by chance during the screening of antidiabetic compounds with KK obese mice that were originally isolated on the basis of hyperglycemia[13,14]. The mouse strain, named KK/Rvd, developed severe RVD. Macroscopic examination of the heart of these mice at 8 weeks of age showed massive fibrosis of the entire right ventricular wall that never extended to the left ventricle (**Fig. 1a**,**b**). This resembles the histopathology of human ARVD. We found that the outer third of the right ventricular wall was replaced by fibrous tissue and that calcification also occurred (**Fig. 1c**,**d**). This degenerative process commenced at 6 weeks of age and was completed by 10 weeks of age. There was some variation in the distribution of affected cardiomyocytes, but penetrance of the phenotype was almost 100%. Histologically, degradation of cardiomyocytes and macrophage infiltration were observed at the border between the fibrosis and the viable myocardial tissue (**Fig. 1e**,**g**), indicating that cardiomyocyte degeneration proceeded from the outer part of the right ventricular wall to the inner part. This outer-inner progression of RVD is also characteristic of human ARVD. Thin fibrous tissue surrounded the degraded cardiomyocytes at the

[1]Department of Internal Medicine and Therapeutics, Osaka University Graduate School of Medicine, 2-2 A8 Yamadaoka, Suita, Osaka 565-0871, Japan. [2]Cardiovascular Division of Internal Medicine, National Cardiovascular Center, 5-7-1 Fujishirodai, Suita, Osaka 565-8565, Japan. [3]Laboratory for Genome Exploration Research Group, RIKEN Genomic Sciences Center (GSC), RIKEN Yokohama Institute, Yokohama, Kanagawa 230-0045, Japan. [4]Department of Gene Therapy Science, Osaka University Graduate School of Medicine, 2-2 Yamadaoka, Suita, Osaka 565-0871, Japan. [5]Department of Nutrition and Physiological Chemistry, Osaka University Graduate School of Medicine, 2-2 Yamadaoka, Suita, Osaka 565-0871, Japan. Correspondence should be addressed to M.K. (kitakaze@zf6.so-net.ne.jp) or S.T. (takasima@medone.med.osaka-u.ac.jp).

Published online 18 January 2004; doi:10.1038/ng1294

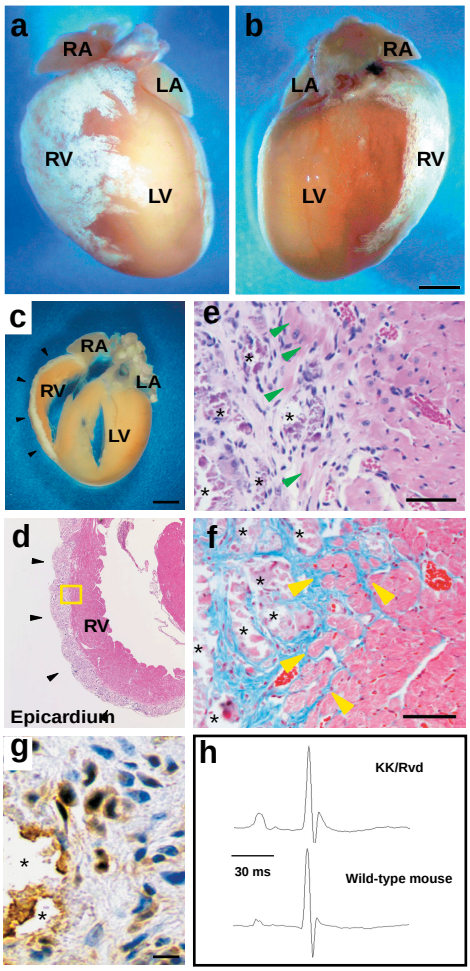

Figure 1 Massive fibrosis covers the outer side of the right ventricular wall, as with human ARVD, and never extends to the left ventricle. Macroscopic view of KK/Rvd mouse heart at 8 weeks old: (**a**) front view, (**b**) back view. (**c**,**d**) In the sagittal section, arrowheads indicate the degenerated area of the right ventricle. (**e**,**f**) At the borderline of the degenerated area (high magnification of yellow square in **d**), green arrows indicate the cardiomyocytes densely stained by eosin; yellow arrows indicate the degraded cardiomyocytes surrounded by fibrous tissue; asterisks indicate calcification. (**e**) Hematoxylin and eosin staining. (**f**) Masson-trichrome staining. (**g**) Infiltrating macrophages into a degraded area are stained by MCP-1 antibody. (**h**) Electrocardiography showed a prolonged QRS duration in KK/Rvd mice. LA, left atrium; LV, left ventricle; RA, right atrium; RV, right ventricle. Scale bars: **a**–**c**, 3 mm; **e**,**f**, 50 μm; **g**, 10 μm.

edge of the myocardial degeneration (**Fig. 1f**), indicating progressive replacement by fibrous tissue.

As lymphocyte infiltration was rarely observed, even when immunohistochemical staining was used (data not shown), autoimmune and infectious mechanisms were probably not involved. Detailed microscopic examination showed that the left ventricular myocardium was intact without any of the changes seen in the right ventricular myocardium. Electrocardiography showed a prolonged QRS duration (duration of ventricular muscle depolarization) in KK/Rvd mice compared with wild-type mice (**Fig. 1h**); this indicated a greater susceptibility to arrhythmia caused by intraventricular conduction disturbance. But electrocardiographic monitoring did not detect tachyarrhythmia, which is often seen in human ARVD. The other organs of these mice showed no histological abnormalities. Thus, KK/Rvd mice matched three of the primary clinical criteria for ARVD[15]: regional right ventricular dysplasia, inheritability and fibro-fatty replacement. Thus we concluded that this was an appropriate mouse model of human ARVD.

Identification of the locus underlying RVD

To investigate the mode of inheritance of RVD, we carried out a cross test between the wild-type PWK mouse strain and the KK/Rvd strain. F_1 mice showed no RVD, whereas the segregation ratio of normal to RVD mice among the F_2 and backcross progeny indicated that RVD was inherited as an autosomal recessive trait. We named the associated locus 'right ventricular dysplasia' (*rvd*). Linkage analysis of these backcross mice ($n = 480$) with the use of 165 microsatellite markers showed that the *rvd* locus was closely linked to *D7Mit270* near the middle of chromosome 7, with a maximum multipoint odds score of 4.67 (**Fig. 2a**). Using other markers deduced from the gene databases flanked with *D7Mit270*, we further genotyped these mice and localized the recombinants to a region of ~3.0 cM.

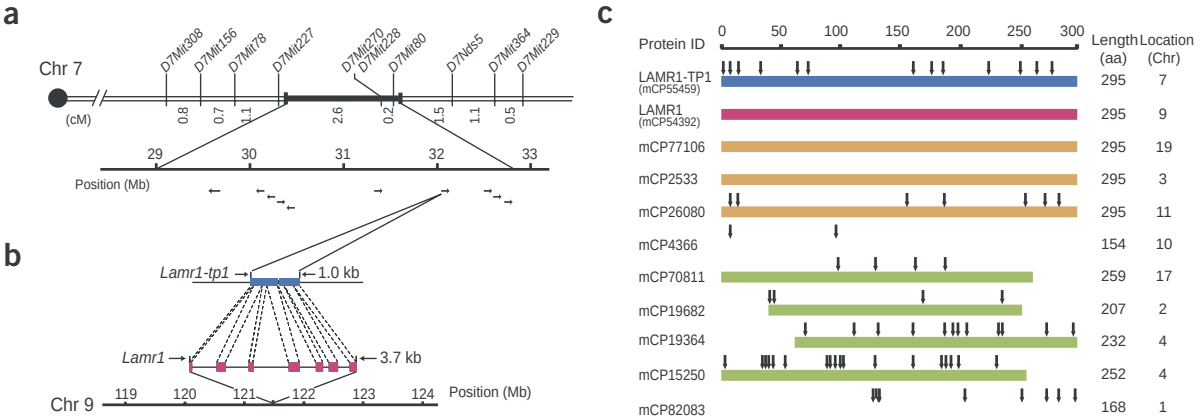

Figure 2 Location, alignment and expression of *Lamr1-tp1*. (**a**) The *rvd* locus was mapped to mouse chromosome 7, linking to *D7Mit270*. (**b**) Sequence of 1,031 bp was inserted in the KK/Rvd mouse genome but not in the PWK mouse genome. (**c**) Alignments of *Lamr1* retroposons in the mouse genome database and the comparison of translated amino acid (aa) sequences to the LAMR1 sequence (from the original *Lamr1* gene located in chromosome 9). Arrows indicate the amino acid transitions.

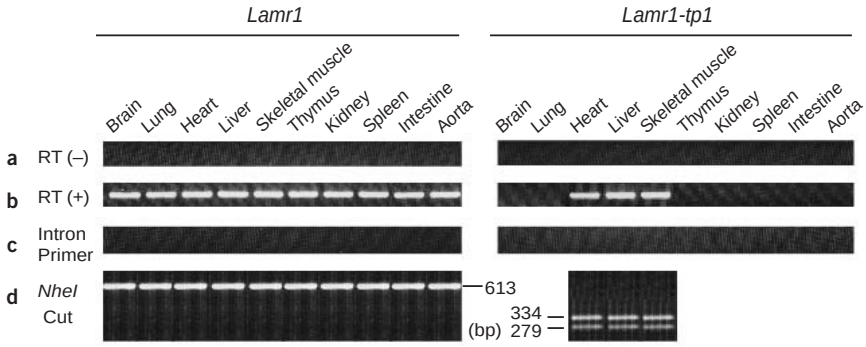

Figure 3 The expression of *Lamr1-tp1* was confirmed only in KK/Rvd heart, liver and skeletal muscle. (**a**) RT(–) indicates the use of RNA samples from KK/Rvd tissues as the PCR template before RT-PCR. PCR primers were designed to include either *Lamr1*- or *Lamr1-tp1*-specific mutated sequences. (**b**) RT(+) indicates the use of the cDNA samples after RT-PCR. The primers were the same as in **a**. (**c**) The same templates were used as in **b**, but reaction primers were designed in the intron lesion of *Lamr1* or up- or downstream of *Lamr1-tp1*. (**d**) PCR products of **b** were digested by the restriction enzyme *Nhe*I, whose recognition site exists only in *Lamr1-tp1*.

Then we sequenced the exons of the *rvd* locus in the gene database and compared the sequences between KK/Rvd and PWK mice. New differences between the two strains shown by this analysis were used as markers to narrow the candidate locus. Within the narrowed region (0.5 cM) we found a 1,031-bp insertion in the KK/Rvd genome that was not present in the PWK genome (**Fig. 2b**). This insert was a 1,031-bp retroposon that encoded mutated *Lamr1*, which we named *Lamr1-tp1* (laminin receptor 1, transposed paralog 1). There was neither an annotated area nor a dbEST matched area within ~1 Mb of this insertion, indicating that alteration of a nearby gene was probably not the cause of this phenotype and suggesting that *Lamr1-tp1* itself was responsible for RVD.

The original *Lamr1* gene consists of seven exons and six introns located on chromosome 9, and it comprises 32 variants of retroposons that are probably derived from a retrovirus. The alignments of these paralogs of *Lamr1* are shown (**Fig. 2c**). Almost all the retroposons have stop codons in the open reading frame and thus are probably not translated. But four *Lamr1* retroposons, including *Lamr1-tp1*, have the stop codon in the same position as the *Lamr1* cDNA. This suggests that these genes could be translated to produce proteins with various mutations. Among the four full-length retroposons, two genes have exactly the same sequence as *Lamr1* and two genes encode mutated *Lamr1* (one of these is *Lamr1-tp1* located on chromosome 7 in KK/Rvd mice and the other is located on chromosome 11). The protein encoded by *Lamr1-tp1* (LAMR1-TP1) shares 96% sequence identity with the protein encoded by *Lamr1* (LAMR1), resulting in the translation of a protein showing a 13–amino acid mutation.

Tissue expression of *Lamr1-tp1*

For *Lamr1-tp1* to cause ARVD, this retroposon would need to be transcribed in the hearts of KK/Rvd mice. We used specific RT-PCR to amplify *Lamr1-tp1* and *Lamr1* transcripts. We isolated RNA and treated it with DNase to eliminate contamination by genomic DNA before RT-PCR. We confirmed the absence of contamination using several PCR reactions with different pairs of intron primers. *Lamr1-tp1* mRNA could only be transcribed in the heart, liver and skeletal muscle of KK/Rvd mice, whereas *Lamr1* mRNA was expressed ubiquitously (**Fig. 3**). Also, *Lamr1-tp1* was not transcribed in any of the tissues of PWK mice or other wild-type (C57Bl/6) mice. There was no difference in the expression of *Lamr1-tp1* in the right ventricle and left ventricle, suggesting that an additional factor was necessary to cause the specific pathological changes associated with ARVD. Despite the high expression of *Lamr1-tp1* transcripts, no pathology was observed in the liver and skeletal muscle of KK/Rvd mice.

In vivo role of LAMR1-TP1

To confirm that the *Lamr1-tp1* transcripts were responsible for the ARVD phenotype, we carried out functional studies of LAMR1-TP1. We transfected a green fluorescent protein (GFP) coexpression plasmid (pIRES2EGFP-Lamr1-tp1 or pIRES2EGFP-Lamr1) into the hearts of C57Bl/6 mice by direct injection of DNA into the right ventricle as described[16]. Three weeks after transfection, we detected expression of LAMR1-TP1 along with massive right ventricular wall damage at the injected area. We observed GFP^+ cardiomyocytes transfected with pIRES2EGFP-Lamr1-tp1 in the zone of degeneration accompanied by fibrosis (**Fig. 4a–c**). The degeneration of transfected cardiomyocytes started 2 weeks after injection of the plasmid. Lymphocyte infiltration was rarely seen in the injected area, and the same changes were also observed in immunosuppressed severe-combined immunodeficient mice (data not shown), suggesting that autoimmunity was probably not involved in this tissue damage. On the other hand, the hearts injected with plasmid pIRES2EGFP-Lamr1

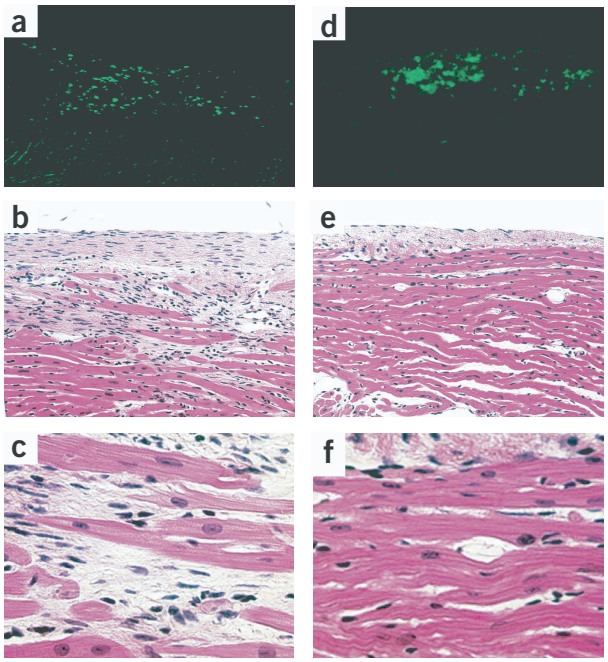

Figure 4 The direct gene injections showed the *Lamr1-tp1*-specific degradation of the myocardium. (**a**,**d**) GFP expression was detected in the gene-injected area. (**b**,**e**) Macroscopic view of transfected sites. (**c**,**f**) Magnified view of the transfected sites. (**a**–**c**) The vector pIRES2EGFP-Lamr1-tp1 was used. (**d**–**f**) The vector pIRES2EGFP-Lamr1 was used. Magnification: **a**,**d**, ×40; **b**,**e**, ×100; **c**,**f**, ×400.

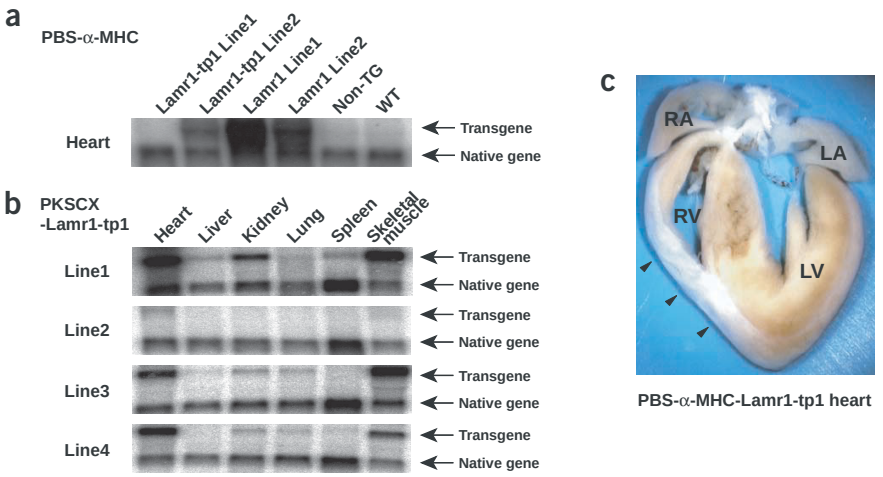

Figure 5 Expressional (northern blot) analysis both of the transgenes and native genes in each transgenic mouse model. *Lamr1-tp1* and *Lamr1* were detected in equal amounts in this analysis. (**a**) Transgene expression in heart samples from two strains of PBS-α-MHC-Lamr1-tp1 mice, two strains of PBS-α-MHC-Lamr1 mice and a control (WT) mouse strain. Non-TG, nontransgenic strain. (**b**) Comparison of gene expression by four lines of the transgenic mouse model PKSCX-Lamr1-tp1 in which transgenes were systemically expressed. (**c**) The complete change to the right ventricle is shown in a macroscopic view of a PBS-α-MHC-Lamr1-tp1 heart from a 10-week-old mouse. LA, left atrium; LV, left ventricle; RA, right atrium; RV, right ventricle.

showed only slight damage at the injection site and the GPF$^+$ cells were healthy, showing no degradation (**Fig. 4d–f**). Fibrous tissue was rarely seen in the hearts transfected with *Lamr1*.

We analyzed further the role of LAMR1-TP1 using transgenic mice. We generated two strains of transgenic mice that expressed *Lamr1* either systemically (with a KSCX promoter) or only in the heart (with an α-MHC promoter). We then established six substrains of *Lamr1-tp1* transgenic mice (four with KSCX promoters and two with α-MHC promoters) and four substrains of *Lamr1* transgenic mice (**Fig. 5a**,**b**). Among the six strains of *Lamr1-tp1* transgenic mice, four strains showed cardiac expression of the LAMR1-TP1 product.

All four strains expressed LAMR1-TP1 in the heart and were extremely susceptible to RVD (**Fig. 5c**). Sometimes the tissue damage extended to the left ventricle, but right ventricle involvement was always predominant. So far, no phenotypic changes have been detected in the other organs of *Lamr1-tp1* transgenic mice. In contrast, all strains that expressed LAMR1 showed no marked changes in any organ, including the heart. These data indicated that LAMR1-TP1 was responsible for RVD in KK/Rvd mice.

In vitro role of LAMR1-TP1

The *in vitro* expression of LAMR1-TP1 also impaired cardiomyocyte function. Cultured rat cardiomyocytes were transfected with an adenovirus vector containing Lamr1-tp1-IRES-GFP and Lamr1-IRES-GFP under the control of a CA promoter. To clarify the effects of these constructs, we carried out an MTS assay. Only expression of *Lamr1-tp1* by cardiomyocytes led to a decrease of cell numbers 48 h after transfection (**Fig. 6a**), even though the same transfection efficiency was confirmed in all groups based on the level of GFP expression (**Fig. 6b**). On histochemical staining, the most prominent change in these cells was alteration of the chromatin architecture. Staining of heterochromatin by DAPI showed a mosaic pattern in cardiomyocytes transfected with *Lamr1* and a speckled pattern in cardiomyocytes transfected with *Lamr1-tp1*.

We analyzed the localization of LAMR1 and LAMR1-TP1 by confocal microscopy. Rat cardiomyocytes transfected with an adenovirus vector were stained using a LAMR1 antibody (FD4818). This antibody could not distinguish LAMR1 from LAMR1-TP1, but only transfected proteins were stained because endogenous LAMR1 was not detected at its relatively low level of expression. LAMR1 was identified in the DAPI-negative euchromatin area of the nucleus, showing a mirror image to the pattern of DAPI staining (**Fig. 6c**). On the other hand, transfection with *Lamr1-tp1* altered the overall pattern of chromatin as described above and LAMR1-TP1 was partially colocalized with the DAPI-positive heterochromatic loci (**Fig. 6c**). These structural changes to chromatin were observed 10–12 h after transfection and preceded the onset of decreasing cell numbers 24 h after transfection.

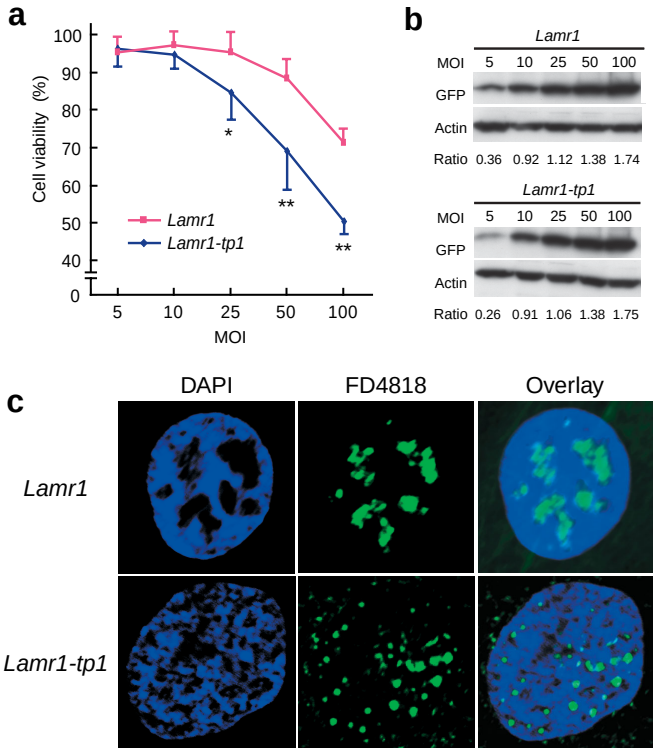

Figure 6 *Lamr1-tp1* caused cardiomyocyte cell death. Cardiomyocytes were infected with recombinant adenoviruses at the indicated multiplicity of infection (MOI). (**a**) Cells expressing *Lamr1-tp1* show lower MTS activity 48 h after adenovirus infection. $*P < 0.05$ versus *Lamr1*; $**P < 0.005$ versus *Lamr1*. (**b**) GFP and actin expression were analyzed 8 h after adenovirus infection. Cell numbers were equivalent at this time point. The ratios of densitometric measurement of GFP:actin are indicated. (**c**) The nuclei of rat cardiomyocytes expressing Lamr1-IRES-GFP or Lamr1-tp1-IRES-GFP were stained with the LAMR1 antibody FD4818 (green) and DAPI (blue). LAMR1 staining showed a perfect mirror image to DAPI-positive area. LAMR1-TP1 was translocated and partially overlapped with DAPI-positive. Scale bar, 20 μm.

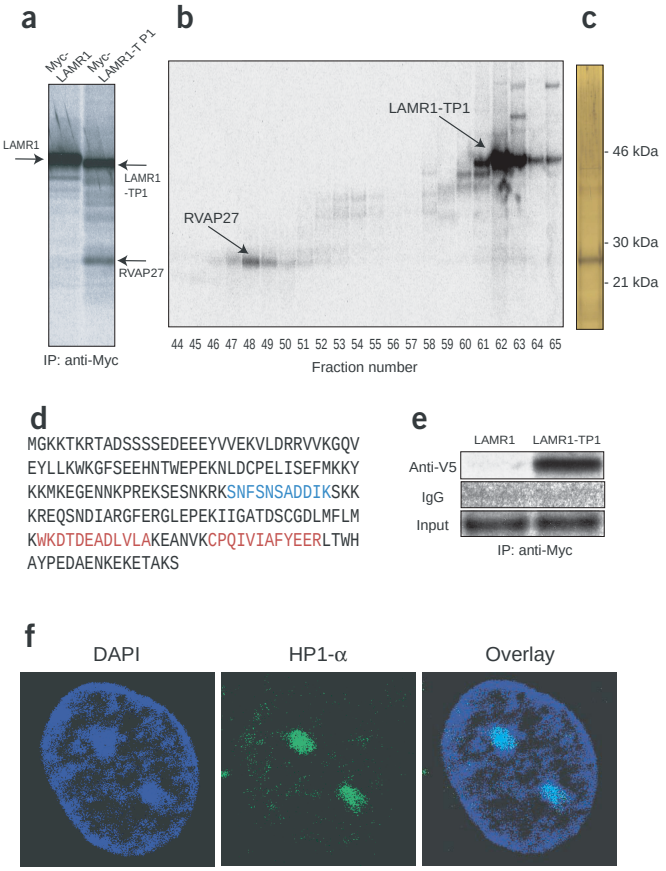

Figure 7 LAMR1-TP1 interacts with HP1-α. (**a**) RVAP27 was immunoprecipitated with LAMR1-TP1 but not with LAMR1 in COS7 cells labeled by ^{35}S-cystein and methionine. (**b**) The complex of radiolabeled LAMR1-TP1 and RVAP27 was separated by a phenyl reverse-phase column. (**c**) The final purification product of RVAP27 was silver-stained. (**d**) The peptides derived from the purified protein, which fitted with those of human HP1-α (as assessed by direct N-terminal sequencing (red) or liquid chromatography-mass spectrometry or mass spectrometry (blue)), are underlined. Cytokine was detected as a Cys-S-propionamide. (**e**) V_5-LAMR1-TP1 but not V_5-LAMR1 expressed in COS7 cells was immunoprecipitated with Myc-tagged HP1-α by anti-Myc. IgG was derived from nonimmunized serum. (**f**) Rat cardiomyocytes were stained with HP1-α antibody, showing HP1-α localization with the DAPI-positive heterochromatin area.

The data suggested that these chromatin changes might have had a lethal effect on the cardiomyocytes, although the possibility that these changes were secondary to lethal cell damage itself cannot be fully excluded.

HP1 binds to mutant LAMR1

To clarify the cellular mechanism by which LAMR1-TP1 caused conformational changes of heterochromatin, we purified and cloned the protein specifically interacting with LAMR1-TP1. The Myc-tagged LAMR1-TP1 fusion protein expressed in ^{35}S-labeled COS7 cells showed the same migration pattern as Myc-tagged LAMR1 (**Fig. 7a**). This 27-kDa protein (named RVAP27) was immunoprecipitated with LAMR1-TP1 but not with LAMR1. Using either a mouse cell line (3T3) or rat cardiomyocytes, we also immunoprecipitated RVAP27 with transfected LAMR1-TP1. Large-scale purification of RVAP27 was done by the sequential use of columns (**Fig. 7b**), and about 10 pmol of RVAP27 was purified from the lysate of 1.0×10^8 COS7 cells (**Fig. 7c**). We analyzed the peptides digested from the RVAP27 band by Edman degradation N-terminal sequencing or nanoelectrospray ionization tandem mass spectrometry. RVAP27 included fragments of the amino acid sequences of SNFSNSADDIK, WKDTDEADLVLA and CPQIVIAFYEER that matched human heterochromatin protein 1-α (HP1-α) (**Fig. 7d**). The Myc antibody coprecipitated Myc-tagged HP1-α with V_5-tagged LAMR1-TP1, but not with LAMR1; this verified the specific interaction between HP1-α and LAMR1-TP1 (**Fig. 7e**).

HP1 is a key heterochromatin protein that regulates gene silencing by interacting with methylated histones[17]. HP1-α also localizes with DAPI-positive heterochromatin[18]. Cardiomyocytes expressing HP1-α showed the same staining pattern in the DAPI-dense region (**Fig. 7f**). Our immunohistochemical data showed that LAMR1 localized to the euchromatin (DAPI-negative) and that LAMR1-TP1 was partially translocated to heterochromatin (DAPI-positive; **Fig. 6c**). These findings imply that the mutant LAMR1 had an increased affinity for HP1-α and thus was translocated to heterochromatin. Such translocation might influence transcriptional regulation and interfere with the expression of genes essential to the survival of cardiomyocytes, leading to lethal cell dysfunction due to LAMR1-TP1.

Changes of gene expression induced by LAMR1-TP1

To investigate transcriptional regulation by LAMR1-TP1, we analyzed changes in gene expression in cultured cardiomyocytes after transfection of *Lamr1-tp1* or *Lamr1*. Because cells expressing *Lamr1-tp1* began to die 24 h after transfection, we analyzed gene expression at 6 h, 12 h and 24 h (each in duplicate) to exclude the secondary effects of lethal cell damage. GFP expression indicated that the transfected protein was expressed 10 h after transfection, indicating that the expression of genes at 6 h was largely induced by viral infection itself. Transfection with wild-type LAMR1 had a minimal effect on the expression profile compared with that of nontransfected cardiomyocytes, even though the adenovirus vector itself should cause some cell damage (**Supplementary Fig. 1** online). On the other hand, LAMR1-TP1 caused substantial changes in gene expression at 12 h and 24 h, but not at 6 h (**Supplementary Table 1** online). These genes showed similar changes in expression in duplicate analyses. We confirmed further the expression of these genes by quantitative PCR (**Supplementary Fig. 1** online). Our results suggested that LAMR1-TP1, but not LAMR1, could alter the expression of some specific genes. How these genes actually determine the fate of cardiomyocytes needs to be determined in order to understand the pathological role of this mutant protein.

DISCUSSION

Although lethal tachyarrhythmia is often detected in human ARVD, we did not detect it in this mouse model. The difficulty in generating lethal tachyarrhythmia in mice, due to the high beating rate and small size of their hearts[19], might explain our failure to detect lethal arrhythmia. KK/Rvd mice showed electric conduction inhomogeneity leading to prolonged QRS duration, which is often seen in humans with ARVD[20,21]. If similar degradation occurs in the human heart, it will become a focus for lethal arrhythmia at some stage in life. The most important pathological feature of ARVD is the degeneration of right ventricular cardiomyocytes[22]. Our ARVD mouse model reproduced the specific right ventricular degeneration from the outside inwards.

It is still not known why the right ventricle is more susceptible than the left ventricle in these mice. Injection of *Lamr1-tp1* into the left ventricle also induced cardiomyocyte degeneration and calcification,

Table 1 Comparison of human *LAMR1* and histone-related gene loci with ARVD loci

ARVD candidate locus	*LAMR1* related gene	Histone-related gene
ARVD4, 2q32.1–32.3	XM_013127*, 2q31	*HAT1*, 2q31.2–33.1
ARVD5, 3p23	*LAMR1*, 3p21	
ARVD6, 10p12–14	XM_053952*, 10p14	

HAT1, histone acetyl transferase 1; asterisks, *LAMR1* retroposons.

but the changes were less severe (data not shown). Also, transgenic mice that expressed LAMR1-TP1 in both cardiac chambers showed predominant right ventricular degeneration. It seems possible that the threshold for cardiomyocyte damage is higher in the left ventricle than in the right ventricle. This implies that a higher level of *Lamr1-tp1* expression could cause left ventricular degeneration. Often in human ARVD, a part of the left ventricle is involved. Although both ARVD2 and Naxos disease show a right ventricle–specific phenotype in humans, the genes responsible are equally expressed in both cardiac chambers[6,23]; the mechanism of right ventricular susceptibility is still unknown. The most likely explanation is that specific genes that determine the susceptibility to cell damage exist in either ventricle. Left ventricular cardiomyocytes are under high stress because of the high pressure in this ventricle, and more cytoprotective genes may be induced as a result. In fact, microarray analysis comparing right ventricle and left ventricle shows higher expression in the left ventricle of genes belonging to the category of cell and organism defense[24]. Dominant degeneration of the outer right ventricular wall in ARVD also supports this concept because the inner free wall is under more mechanical stress and expresses more defensive genes, such as heat shock proteins. This mechanism might lead to left ventricle protection in ARVD. Alternatively, right ventricle–specific genes may be involved in the susceptibility of the right ventricle. Mice lacking the right ventricle–specific gene actinin-associated LIM-domain protein show some ARVD-like features[25], even though the histological characteristics are considerably different from those of human ARVD.

We found that one of the heterochromatin complex proteins, HP1-α, showed specific binding to LAMR1-TP1. HP1-α is a key component of condensed DNA and is involved in gene silencing by interaction with methylated histone H3. Mobility of HP1-α has been reported in various cells[18,26]. The stochastic competition between such factors as LAMR1-TP1 and HP1-α may determine the fate of the heterochromatin plasticity that is involved in regulating the fate of cells. Class II histone deacetylase acts as a signal-responsive suppressor of the transcriptional events governing cardiac hypertrophy and heart failure[27]. HP1 can link with class II histone deacetylase[28] and thus may modify cardiac cell metabolism. Accordingly, we conclude that LAMR1-TP1 was translated from an active retroposon in ARVD mice and then interacted with HP1-α, leading to the early death of cardiomyocytes.

Genomic databases indicate that there are up to 40 and 32 *Lamr1* retroposons in humans and mice, respectively. It has also been suggested that the *Lamr1* gene family in mammals, with the exception of the functional locus, is comprised entirely of retrotransposons or processed pseudogenes. Most processed retroposons are not expressed and have no functional activity, but several active retroposons or pseudogenes have been identified[29–32]. We show that the active retroposon may cause the pathological condition of ARVD. In humans, a highly conserved mutated form of *Lamr1* has been isolated from a fetal brain cDNA library[33], suggesting that mutant LAMR1 proteins are also transcribed in humans. Several reported human ARVD loci are located close to the retroposons of *Lamr1* or histone-modulating protein genes (**Table 1**), suggesting that either LAMR1 or HP1 may cause hereditary RVD in humans.

METHODS

PWK mouse strain. The PWK strain belongs to the *Mus musculus musculus* subspecies, which separated from *Mus musculus domesticus* some 1 million years ago. It is maintained as one of the wild-type–derived inbred strains.

***Lamr1-tp1* expressional analysis.** We carried out PCR assays to confirm the presence of each identified mutation. Mismatch assays for the 287T→C and 291G→T mutations in the nucleic acid sequence of *Lamr1* introduced changes at the penultimate 3′ position for the forward primer and 868C→T for the reverse primer, respectively (primer sequences available on request). Each PCR product was digested with *Nhe*I (specific for *Lamr1-tp1* amplicon) to produce fragments of 334 bp and 279 bp; the *Lamr1* amplicon was uncut.

Injection of recombinant DNA *in vivo*. Female C57Bl/6 mice (8 weeks old, 22–25 g) were anesthetized with a mixture of ketamine (100 mg per kg body weight intraperitoneally) and xylazine (5 mg kg body weight intraperitoneally), intubated and ventilated. We carried out a left lateral thoracotomy to expose the beating heart and injected 10 μg of plasmid DNA in 100 μl of phosphate-buffered saline containing 5% sucrose into the right ventricular wall with a 30-gauge needle. The mice were killed 3 weeks after injection and histological staining was done.

Transgenic mice models. We constructed three kinds of targeting vectors under the following promoters (*Lamr1-tp1*, KSCX and α-MHC; *Lamr1*, α-MHC). We introduced these targeting vectors into blastocysts (derived from the C57Bl/6 Jcl mouse strain) by a standard pronuclear microinjection technique[34].

Preparation of adenovirus. Replication-defective recombinant adenoviral vectors expressing Lamr1-tp1-IRES-GFP and Lamr1-IRES-GFP were prepared with the adenovirus expression vector kit following the manufacturer's protocol (Takara). Briefly, *Lamr1-tp1* and *Lamr1* cDNA connected to an IRES-GFP sequence (Clontech) were placed after a CA promoter that was composed of a cytomegalovirus enhancer; a chicken β-actin promoter and rabbit β-globin poly(A) were inserted into a cassette cosmid vector that contained an entire adenovirus type 5 genome except for the E1a, E1b and E3 regions. A recombinant adenovirus was constructed by *in vitro* homologous recombination in HEK293 cells with the use of this cosmid vector and the adenovirus DNA terminal-protein complex. The desired recombinant adenovirus was purified by ultracentrifugation through a $CsCl_2$ gradient followed by extensive dialysis. The titer of the virus stock was assessed by a plaque formation assay that used the HEK293 cells. Cardiomyocytes were infected with the recombinant adenovirus vectors at a multiplicity of infection of 5–100 plaque-forming units per cell. We assessed the expression of GFP and β-actin by immunoblotting with 20 μg of myocardial protein lysate.

Primary culture of neonatal rat ventricular myocytes and MTS assay. Ventricular myocytes obtained from 1- or 2-d-old Wister rats were prepared and cultured overnight in Dulbecco's modified Eagle medium containing 10% fetal bovine serum as described[35]. Cytotoxicity was assessed with a CellTiter 96 Aqueous One Solution Cell Proliferation Assay System (Promega). Rat cardiomyocytes were cultured in 96-well culture plates at a density of 3×10^4 cells cm^{-2}. MTS reagent was added to each well 48 h after the addition of adenovirus to the myocytes. After a 1-h incubation period, optical absorbance at 490 nm was measured with a microplate reader. Cell viability was expressed as mean percentages for the absorbance at multiplicity of infection of 5 with the standard deviations of absorbance.

Antibodies. We used antibodies to MCP-1 (Santa Cruz Biotechnology), GFP, Myc-conjugate beads (Clontech), V_5 (Invitrogen) and HP1-α (Upstate Biotechnology). The polyclonal antibody FD4818 was derived from rabbits against the amino acid sequence RALNVLQMKEEDVFK, which corresponds to amino acids 3–15 of LAMR1.

Identification of LAMR1-TP1 binding protein (RVAP27). We metabolically labeled 2.0×10^5 COS7 cells expressing either PCDNA3.1-Myc-tagged-Lamr1 or PCDNA3.1-Myc-tagged-Lamr1-tp1 (Invitrogen) with ^{35}S, lysed them with 1 ml of lysis buffer (20 mM Tris pH 8.0, 5% acetonitrile, 5 M MEDTA, 1% Nonidet P-40) and immunoprecipitated them with a Myc antibody. Bound materials were separated by SDS-PAGE and the radioactivity was detected by a BAS imaging analyzer (Fuji). The eluted fraction from Myc-antibody beads was also injected onto a Phenyl-RPLC column (4.6 × 250mm, Nakarai) equilibrated with 0.1% trifluoroacetic acid and 5% acetonitrile. Fractions were eluted with a linear gradient of 27–37% acetonitrile at a flow rate of 1 ml. Each fraction was lyophilized and separated by SDS-PAGE. Radioactivity was detected by BAS imaging system.

Large-scale purification and sequence analysis of LAMR1-TP1–binding protein. COS7 cells (1.0×10^8) expressing Myc-tagged LAMR1-TP1 were lysed with 200 ml of lysis buffer and applied to 500 µl of Myc-antibody beads (Clontech). Bound materials were eluted with 0.1% trifluoroacetic acid and 5% acetonitrile. The eluted fraction was diluted 50 times with a lysis buffer and was applied to Uno-Q anion exchange column (Bio-Rad). The column was equilibrated with 20 mM Tris and 5% acetonitrile at pH 8.0 and bound materials were eluted with a linear gradient of NaCl (0–0.5 M) at a flow rate of 1 ml min^{-1}. Five fractions of about 0.3 M NaCl elution were pooled and injected onto a Phenyl-RPLC column (4.6 × 250 mm, Nakarai) equilibrated with 0.1% trifluoroacetic acid and 5% acetonitrile. Fractions were eluted with a linear gradient of 27–37% acetonitrile at a flow rate of 1 ml. After separating by SDS-PAGE, RVAP27 was eluted at the same fraction in which the radioactive LAMR1-TP1 was detected. Purified RVAP (10 pmol) was subjected to SDS-PAGE on 12% gel. After staining the gel with SyproRuby, the 27-kDa band was cut and treated with trypsin. The tryptic digest was fractionated by nanoscale HPLC on a C18 column (0.1 × 50 mm). Two fractions were analyzed by direct N-terminal sequence by Edman degradation with the HP G1005 Protein Sequencing System. One fraction was analyzed with a tandem mass spectrometer (Q-Tof2) equipped with a nanoelectrospray ionization source. Positive ion tandem mass spectra were measured.

RNA preparation and hybridization to oligonucleotide arrays. Total RNA was isolated from viable mice or cultured neonatal cardiomyocytes derived from C57Bl/6 mice. Affymetrix Gene Chip technology was used as described[36]. Briefly, cDNA was synthesized from total RNA and annealed to a T7-oligo-dT primer. Reverse transcription was done with Superscript II reverse transcriptase. Second-strand cDNA synthesis was done with DNA polymerase I with the appropriate reagents. Synthesis of biotin-labeled cRNA was done by *in vitro* transcription with the MEGAscript T7 IVT Kit (Ambion, Inc). The cRNA was fragmented and hybridized to GeneChip Murine U74vA2 Array Set (Affymetrix). Hybridization, probe washing, staining and probe array scan were done according to the protocols provided by Affymetrix. Detailed information about the array protocol and data is available in the GEO database (see URL and accession number below).

Real-time PCR. Real-time PCR was done with TaqMan technology and the ABI Prism 7700 Detection System (Applied Biosystems). Reactions (25 µl) were set up using the 2× Universal PCR Master Mix (Applied Biosystems), template cDNA and adequate concentrations of primers and probes. All of the samples were processed in duplicate. To standardize the quantity of the two selected genes, GAPDH was used as the endogenous control reference because our microarray analysis showed that the level of GAPDH was stable and no significant difference was noted among all the three groups.

Data analysis. GeneSpring 5.0 (Silicon Genetics) software was used for analyses. A global normalization was used for all data in the 18 arrays with a combination of three steps: transforming negative values to 0.01, normalizing to the 50th percentile per chip and normalizing to median per gene. We filtered data using a combination of signal confidence ('present' flag), relative change (1.5–2.0 times), minimum acceptable signal intensity (average difference ≥50 in at least one of three groups) and a statistical cut-off ($P < 0.05$, Student's *t*-test). Data are presented as mean or mean ± s.e.m.; the one-way ANOVA with Tukey-Kramer exact probability test was used to test the differences among all the groups and the least-squares method was used to determine linear correlation between selected variables. $P < 0.05$ was considered statistically significant.

Animal experiments. All animal experiments were approved by the Institutional Animal Care and Use Committee at Osaka University Graduate School of Medicine.

URL. The GEO database is available at http://www.ncbi.nlm.nih.gov/geo/.

GEO accession number. GSE927.

Note: Supplementary information is available on the Nature Genetics website.

ACKNOWLEDGMENTS

These data were generated through the use of the Celera Discovery System and Celera Genomics' Associated Databases. We thank T. Tanaka and K. Miyake for assistance with DNA sequencing; S. Hirota for histologic expertise; H. Niwa for donating plasmid constructs and providing suggestions; K. Yamamoto for amino-acid sequencing; and H. Kikutani, K. Node and T. Nakagawa for discussions. This work was supported by Grants-in-aid for Scientific Research from the Japanese Ministry of Education, Culture, Sports, Science and Technology and from the Ministry of Health and Labor and Welfare, Japan.

COMPETING INTERESTS STATEMENT

The authors declare that they have no competing financial interests.

Received 20 November; accepted 29 December 2003
Published online at http://www.nature.com/naturegenetics/

1. Thiene, G. *et al.* Arrythmogenic right ventricular cardiomyopathy. *Trends Cardiovasc. Med.* **7**, 84–90 (1997).
2. Severini, G.M. *et al.* A new locus for arrhythmogenic right ventricular dysplasia on the long arm of chromosome 14. *Genomics* **31**, 193–200 (1996).
3. Rampazzo, A. *et al.* ARVD4, a new locus for arrhythmogenic right ventricular cardiomyopathy, maps to chromosome 2 long arm. *Genomics* **45**, 259–263 (1997).
4. Ahmad, F. *et al.* Localization of a gene responsible for arrhythmogenic right ventricular dysplasia to chromosome 3p23. *Circulation* **98**, 2791–2795 (1998).
5. Li, D. *et al.* The locus of a novel gene responsible for arrhythmogenic right- ventricular dysplasia characterized by early onset and high penetrance maps to chromosome 10p12-p14. *Am. J. Hum. Genet.* **66**, 148–156 (2000).
6. Tiso, N. *et al.* Identification of mutations in the cardiac ryanodine receptor gene in families affected with arrhythmogenic right ventricular cardiomyopathy type 2 (ARVD2). *Hum. Mol. Genet.* **10**, 189–194 (2001).
7. Bright, J.M. & McEntee, M. Isolated right ventricular cardiomyopathy in a dog. *J. Am. Vet. Med. Assoc.* **207**, 64–66 (1995).
8. Simpson, K.W., Bonagura, J.D. & Eaton, K.A. Right ventricular cardiomyopathy in a dog. *J. Vet. Intern. Med.* **8**, 306–309 (1994).
9. Fox, P.R., Maron, B.J., Basso, C., Liu, S.K. & Thiene, G. Spontaneously occurring arrhythmogenic right ventricular cardiomyopathy in the domestic cat: A new animal model similar to the human disease. *Circulation* **102**, 1863–1870 (2000).
10. Ishikawa, S., Zu Rhein, G.M. & Gilbert, E.F. Uhl's anomaly in the mink. Partial absence of the right atrial and ventricular myocardium. *Arch. Pathol. Lab. Med.* **101**, 388–390 (1977).
11. Sato, M. *et al.* Analysis of nuclear localization of laminin binding protein precursor p40 (LBP/p40). *Biochem. Biophys. Res. Commun.* **229**, 896–901 (1996).
12. Kaneda, Y. *et al.* The induction of apoptosis in HeLa cells by the loss of LBP-p40. *Cell Death Differ.* **5**, 20–28 (1998).
13. Kondo, K., Nozawa, K., Tomita, T. & Ezaki, K. Inbred strains resulting from Japanese mice. *Bull. Exp. Anim.* **6**, 107–112 (1967).
14. Nakamura, M. & Yamada, K. Studies on a diabetic (KK) strain of the mouse. *Diabetologia* **3**, 212–221 (1967).
15. McKenna, W.J. *et al.* Diagnosis of arrhythmogenic right ventricular dysplasia/cardiomyopathy. Task Force of the Working Group Myocardial and Pericardial Disease of the European Society of Cardiology and of the Scientific Council on Cardiomyopathies of the International Society and Federation of Cardiology. *Br. Heart J.* **71**, 215–218 (1994).
16. Lin, H., Parmacek, M.S., Morle, G., Bolling, S. & Leiden, J.M. Expression of recombinant genes in myocardium in vivo after direct injection of DNA. *Circulation* **82**, 2217–2221 (1990).
17. Nakayama, J., Rice, J.C., Strahl, B.D., Allis, C.D. & Grewal, S.I. Role of histone H3 lysine 9 methylation in epigenetic control of heterochromatin assembly. *Science* **292**, 110–113 (2001).
18. Festenstein, R. *et al.* Modulation of heterochromatin protein 1 dynamics in primary Mammalian cells. *Science* **299**, 719–721 (2003).
19. Cranefield, P. *The Conduction of the Cardiac Impulse* (Futura, Mount Kisco, New York, 1975).
20. Peters, S. & Trummel, M. Diagnosis of arrhythmogenic right ventricular dysplasia-cardiomyopathy: value of standard ECG revisited. *Ann. Noninvasive Electrocardiol.* **8**, 238–245 (2003).

21. Nasir, K. *et al.* Filtered QRS duration on signal-averaged electrocardiography predicts inducibility of ventricular tachycardia in arrhythmogenic right ventricle dysplasia. *Pacing Clin. Electrophysiol.* **26**, 1955–1960 (2003).
22. Burke, A.P., Farb, A., Tashko, G. & Virmani, R. Arrhythmogenic right ventricular cardiomyopathy and fatty replacement of the right ventricular myocardium: are they different diseases? *Circulation* **97**, 1571–1580 (1998).
23. Protonotarios, N. *et al.* Genotype-phenotype assessment in autosomal recessive arrhythmogenic right ventricular cardiomyopathy (Naxos disease) caused by a deletion in plakoglobin. *J. Am. Coll. Cardiol.* **38**, 1477–1484 (2001).
24. Steenman, M. *et al.* Transcriptomal analysis of failing and nonfailing human hearts. *Physiol. Genomics* **12**, 97–112 (2003).
25. Pashmforoush, M. *et al.* Adult mice deficient in actinin-associated LIM-domain protein reveal a developmental pathway for right ventricular cardiomyopathy. *Nat. Med.* **7**, 591–597 (2001).
26. Cheutin, T. *et al.* Maintenance of stable heterochromatin domains by dynamic HP1 binding. *Science* **299**, 721–725 (2003).
27. Zhang, C.L. *et al.* Class II histone deacetylases act as signal-responsive repressors of cardiac hypertrophy. *Cell* **110**, 479–488 (2002).
28. Zhang, C.L., McKinsey, T.A. & Olson, E.N. Association of class II histone deacetylases with heterochromatin protein 1: potential role for histone methylation in control of muscle differentiation. *Mol. Cell. Biol.* **22**, 7302–7312 (2002).
29. McCarrey, J.R. & Thomas, K. Human testis-specific PGK gene lacks introns and possesses characteristics of a processed gene. *Nature* **326**, 501–505 (1987).
30. Gebara, M.M. & McCarrey, J.R. Protein-DNA interactions associated with the onset of testis-specific expression of the mammalian Pgk-2 gene. *Mol. Cell. Biol.* **12**, 1422–1431 (1992).
31. Dahl, H.H., Brown, R.M., Hutchison, W.M., Maragos, C. & Brown, G.K. A testis-specific form of the human pyruvate dehydrogenase E1 α subunit is coded for by an intronless gene on chromosome 4. *Genomics* **8**, 225–232 (1990).
32. Hirotsune, S. *et al.* An expressed pseudogene regulates the messenger-RNA stability of its homologous coding gene. *Nature* **423**, 91–96 (2003).
33. Richardson, M.P., Braybrook, C., Tham, M., Moore, G.E. & Stanier, P. Molecular cloning and characterization of a highly conserved human 67- kDa laminin receptor pseudogene mapping to Xq21.3. *Gene* **206**, 145–150 (1998).
34. Gordon, J.W., Scangos, G.A., Plotkin, D.J., Barbosa, J.A. & Ruddle, F.H. Genetic transformation of mouse embryos by microinjection of purified DNA. *Proc. Natl. Acad. Sci. USA* **77**, 7380–7384 (1980).
35. Simpson, P., McGrath, A. & Savion, S. Myocyte hypertrophy in neonatal rat heart cultures and its regulation by serum and by catecholamines. *Circ. Res.* **51**, 787–801 (1982).
36. Lockhart, D.J. *et al.* Expression monitoring by hybridization to high-density oligonucleotide arrays. *Nat. Biotechnol.* **14**, 1675–1680 (1996).